Available online at www.sciencedirect.com
SCIENCE DIRECT
OCEAN ENGINEERING
Ocean Engineering 32 (2005) 1174–1198
www.elsevier.com/locate/oceaneng

Remotely sensing in detecting the water depths and bed load of shallow waters and their changes

Li-Guang Leu[a,*], Heng-Wen Chang[b]

[a]Department of Marine Science, Chinese Naval Academy, P.O. Box 90175, Tsoying, Kaohsiung 813, Taiwan, ROC
[b]Energy & Resources Laboratories, Industrial Technology Research Institute, Hsinchu, Taiwan, ROC

Received 22 October 2004; accepted 7 December 2004
Available online 14 March 2005

Abstract

Bed load is a type of sand drift and accumulation on the sea-bed. Sand drift is a very important index to survey the erosion or deposition of coastal zone. The change of water depths indicates the change of bed load in shallow waters. The conventional method for measuring water depth uses the shipboard echo sounder, which is accurate for point-measurement, but is a time-consuming and labor-intensive task. For periodic survey of bathymetry as synoptic scale, the remote sensing method may be a viable alternative. Wave spectrum bathymetric (WSB) method takes advantages of remote sensing to obtain the bathymetry of shallow waters safely, economically and quickly. The WSB method is feasible to detect the change of water depths over coastal zones where water depths are less than about 12 m. This remote sensing method is worthy to be well developed and efficiently applied to change detection of water depths and bed load in shallow waters.

Keywords: Wave spectrum; Water depth; Bed load; Sand drift; Bathymetry; Change detection

1. Introduction

The bathymetry of coastal waters is of vital importance to coastal ocean engineering projects as well as the shipping safety. The conventional method for measuring water depths uses the shipboard echo sounder, which is accurate for point-measurement, but is a time-consuming and labor-intensive task. For periodic survey of bathymetry at synoptic scale,

* Corresponding author.
E-mail address: lgleu@cna.edu.tw (L.-G. Leu).

0029-8018/$ - see front matter
doi:10.1016/j.oceaneng.2004.12.005

the remote sensing method may be a viable alternative. There are several indirect methods for remotely sensing water depths. One is the optical bathymetry method, which is based on the principles that the total reflected energy of electromagnetic waves from a water column (including the water surface, the water body and the sea bottom) varies with the water depth. Actually, the reflectivity of visible light depends on the quality of the water column and the type of sea floor; the depth of highly turbid water is difficult to be determined by the optical bathymetry method (Hengel and Spitzer, 1991; Tripathi and Rao, 2002). Other methods use radar, such as Synthetic Aperture Radar (SAR), or Side Looking Airborne Radar (SLAR) images to derive the bathymetry of near shore with fairly good results (Kasischke et al., 1983; Alpers and Hennings, 1984; Vogelzang, 1992). Variation in bathymetry or texture of the sea floor under a strong tidal current induces spatial variation of the sea surface roughness. Therefore, studying the backscattered radar intensity along with simultaneous data of wind speed and surface water velocity allows us to determine the sea bottom features under all weather conditions. Generally, the field observation part of this method is relatively difficult to carry out. In this study, an indirect method of remote sensing is applied to determine the water depths and to overcome problems described above. As waves propagate onshore, their wavelengths decrease with water depths in the coastal zone. Therefore, the two-dimensional wavenumber spectrum may be used to derive the water depth. A method has been developed to obtain the bathymetry of shallow waters from wave spectra (Leu, 1998; Kuo et al., 1999). This method is called the Wave Spectrum Bathymetric (WSB) method. The goal of this study is to adopt the WSB method mapping bathymetry of shallow waters and detecting the change of water depths and bed load in coast zone.

In order to use the WSB method to derive the bathymetry of the coastal zone, one has to start by analyzing the wave field. Remote sensing techniques used to observe the water surface waves rely on spatial measurement. In the early development of this method, photography was used to detect the water waves (Cox and Munk, 1954). Since US launched the satellite SEASAT in 1978, SAR images were used to observe sea surface waves (Beal, 1980). The French satellite, Systeme Pour l'observation de la Terre (SPOT) has a visible sensor that provides high-resolution images of surface waves. Unlike the optical bathymetry method where the sensitively is affected by the water quality and the bottom reflectivity, the WSB method is especially suitable for estimating water depths in the west of Taiwan where water quality varies in a short distance. In this paper, two SPOT images over Taichung Harbor (Fig. 1) are analyzed for the spatial distribution of their wavenumber spectra. Assuming that the frequency of wave does not change, and the general dispersion relation between the water depth and the wavelength holds during the wave propagation, we may determine the coastal water depths from the spatial variation of the wave spectra. This WSB method has feasible application because it does not depend on other environmental data, like the water quality and bottom reflectivity for the optical method, and the simultaneously observed wind speed and surface current velocity for analyzing radar images. Vesecky and Stewart (1982) suggest that waves will not be imaged by SAR if the significant waveheight is less than 1.4 m. Generally, the good result of WSB method can be derived from the visible imageries with high spatial resolution and clear wave pattern. Further, by analyzing multi-temporal images, this WSB method could be applied to detect the water depths and bed load accumulated in coastal zone and their changes.

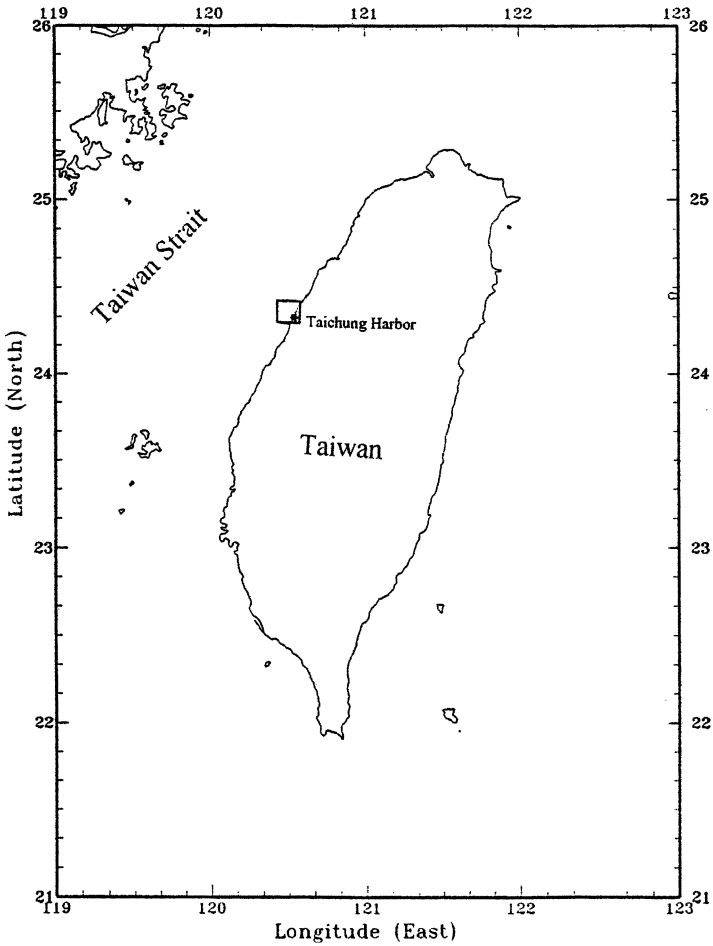

Fig. 1. Map of Taiwan and the area of SPOT images shown as the small square and Taichung Harbor marked as an asterisk.

2. Imagery data and research scope

SPOT is a French satellite of average altitude 832 km, which flies over Taiwan at about 10:45 a.m. To simplify the indexing of its images, SPOT uses its self-defined Grid Reference System (GRS) with values of (K, J) to represent the location of the image over the globe. It lays 369 tracks over the globe and the same track will be repeated every 26 days, which means that SPOT can observe the same area on the globe at the same angle once every 26 days. SPOT has two high-resolution visible sensor systems, and each sensor system has both the multi-spectral (XS) and the panchromatic (PAN) operation modes. This research uses SPOT 3 Geocoded level 10 panchromatic images after geometric correction with ground control points and re-sampling. All pixels are close to square with a size of 6.25 m$\times$6.25 m. These images were corrected to have the upper direction of the images in the northerly direction. Two SPOT images cover the area between the north groin and the north breakwater. One image (Fig. 2a) was taken on March 4, 1994; the other (Fig. 2b) was taken on September 2, 1995.

The study area is located between the north groin and the north breakwater of Taichung Harbor. The reference area is located at 6–7 km offshore with water depth about 50 m (shown in Fig. 2a). In long-term statistics, the waves have a period about 4–6 s over the sea area of Taichung Harbor. Their significant wave heights are almost below 3 m. The contours of bathymetry in shallow water parallel the coastal line of Taichung Harbor. The water depth is about 20 m at the top of the north breakwater and water depths change gradually to 40 m about 4 km. Generally, water depths are about 40–50 m in the open ocean of Taiwan strait.

The spatial change in depth may manifest itself in the wavenumber spectra if its spatial scale is larger than the wavelength. Any drastic change in the water depth can be not accurately reflected in the satellite images of wave crests and troughs. We selected the coastal region of Taichung Harbor for the test of the WSB method, because

(1) the bottom slope is relatively gentle—satisfy the requirement of the WSB method;
(2) the heavy sedimentation near the coast has changed the water depth—a region that needs frequent charting of the bathymetry;
(3) generally, the winter monsoon generates steady swell of periods 4–7 s, and wave height up to 3 m—appropriate for the WSB method in deriving the wavenumber spectra;
(4) routine survey was performed by Taichung Harbor authority—field data is available for the validation of the WSB method.

The water depth is about 20 m at the tip of the north breakwater, and is about 40 m at 4 km offshore. To the western sea area of Taichung Harbor, this area belongs to Taiwan Strait and all its water depths are almost about 40–50 m. To basic assumption, the wave field is regarded homogeneous in reference area of deep water. Its frequency of the dominant wave system keeps constrained while it propagates from deep waters into shallow waters. According to this assumption and principle, the bathymetry of study area in shallow waters can be estimated and charted.

3. Methodology and its application

There are two steps in determining the coastal water depths from SPOT images. The first step is the wave spectrum analysis in both the deep and shallow water regions. The dominant wave in these two regions is assumed to have the same frequency, though different wavenumbers. The second step is the analysis for deriving the water depth.

The water wave retains its frequency while propagating from the deep-water region into the shallow. Inserting this known frequency and the dominant wavenumber in the wavenumber spectrum analysis of coastal wave images, into the general dispersion

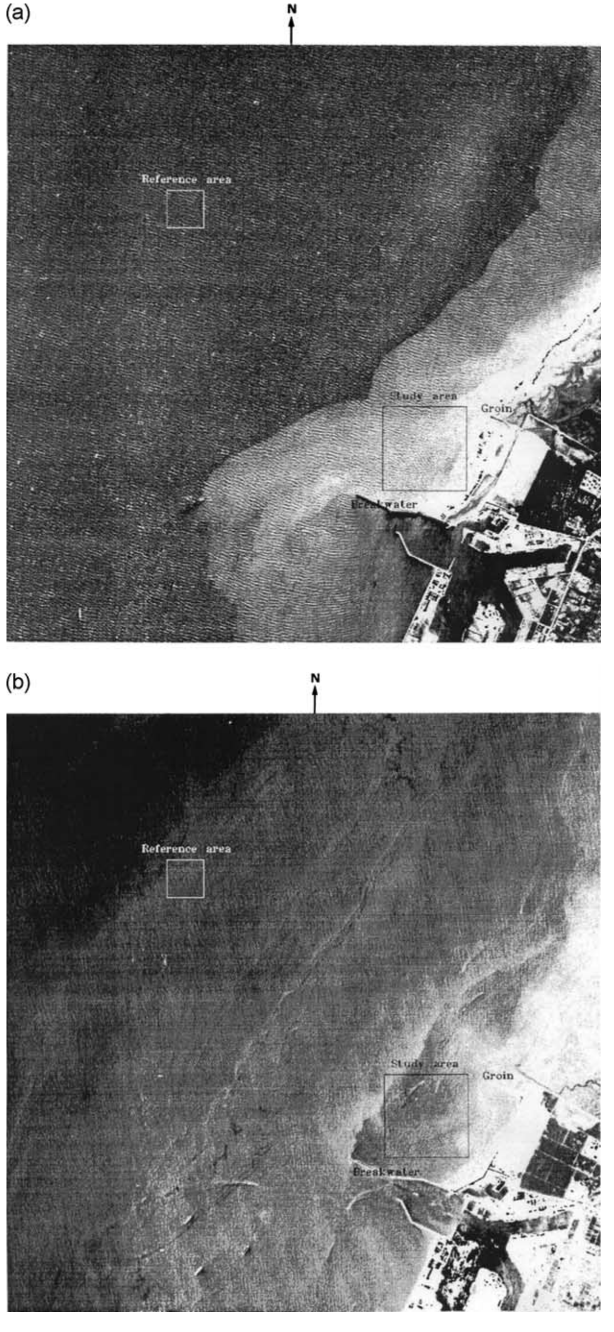

Fig. 2. (a) Case 1: SPOT 3 image on March 4, 1994 over Taichung Harbor, Taiwan. The north is in the upward direction. Copyright@CNES. (b) Case 2: SPOT 3 image on September 2, 1995 over Taichung Harbor, Taiwan Copyright@CNES.

relation of surface waves:

$$(2\pi f)^2 = gk \tanh(kh) \tag{1}$$

We may map the water depths in the coastal zones. At last, we also detect and determine the change of water depths and bed load by analyzing multi-temporal imageries. The flowchart of the analysis is shown in Fig. 3.

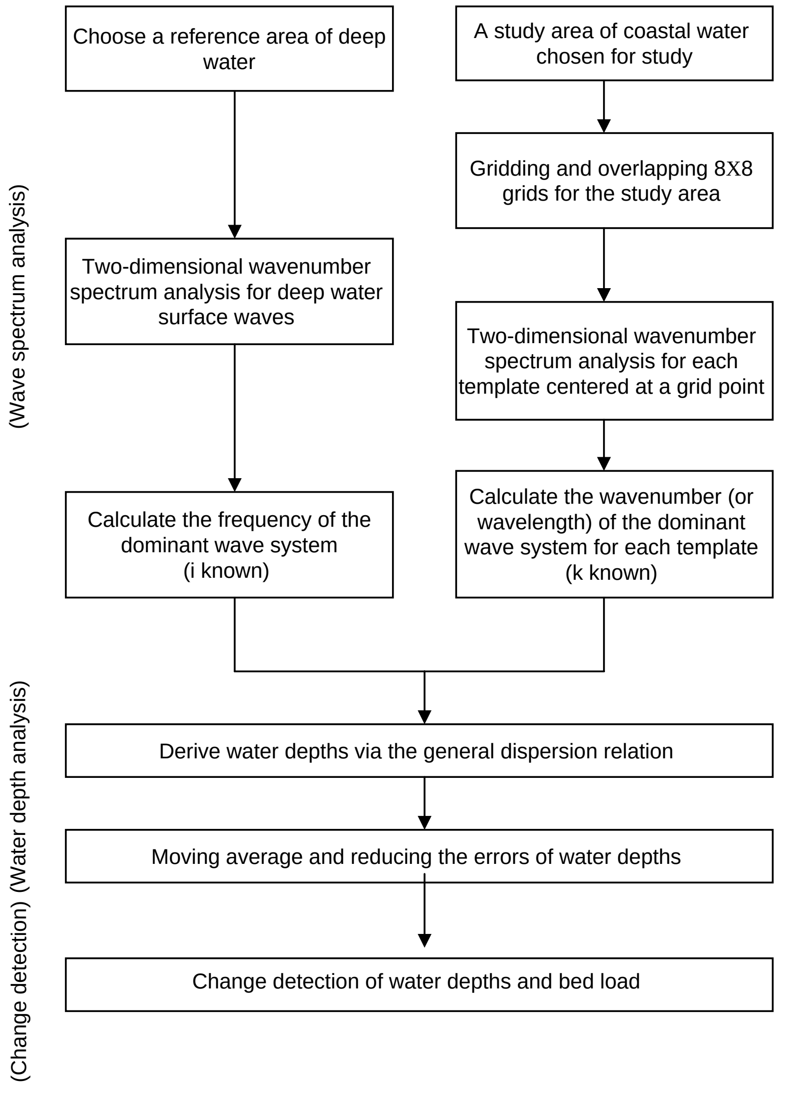

Fig. 3. The flowchart of the change detection and analysis of water depths and bed load by wave spectrum bathymetric method.

3.1. Wave spectrum analysis

Select both a 'reference area' (800×800 m or 128×128 pixels) in the deep-water region of SPOT image and a 'study area' (1800×1800 m) near the coast to perform the wave spectrum analysis and determine the wavenumber of the dominant wave system. From the wavenumber spectrum analysis of waves in the deep-water region, the dispersion relation for deep-water waves may determine the frequency of the surface wave f

$$(2\pi f)^2 = gk \quad k = (2\pi)/\lambda \tag{2}$$

In these two formulas, g is the gravitational acceleration (9.8 m/s/s), k is the wavenumber, and λ is the wavelength. This frequency f is assumed to be the same for waves in both the deep and the shallow regions.

Over the study area, we lay a grid of 8×8 (Fig. 4), with 32 pixels (200 m) between two neighboring grid points, and every cell has 32×32 pixels. For each grid point, we form a template of 64×64 pixels. Each template centers at a grid point and contains four cells. The dominant wave number in this template is determined by its wavenumber spectra.

Because the template dimension is twice the distance between the grid points, there are overlaps among the templates. Furthermore, the computed dominant wavelengths and wave directions are partially related. Therefore, it is smoother across the templates than

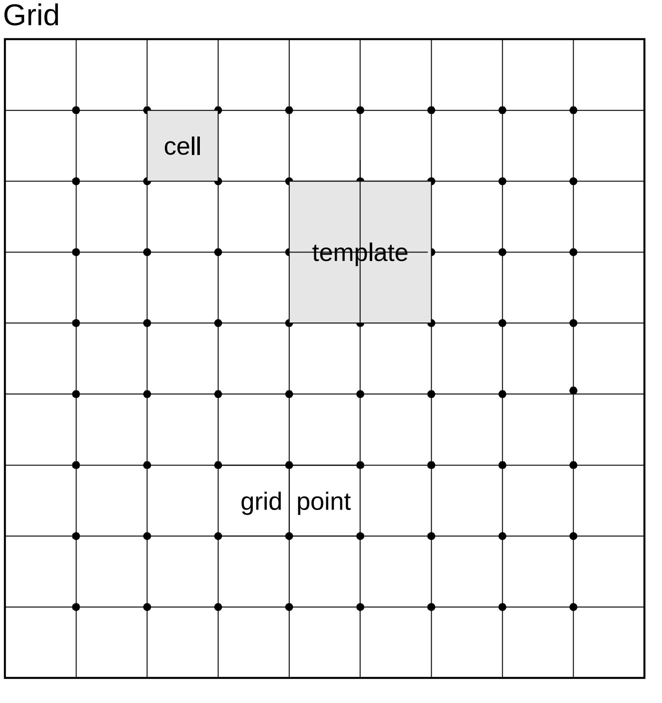

Fig. 4. The grid system of 8×8, laid on the study area, was used in the wave spectrum analysis.

the case of non-overlapping templates. The advantage of using overlapping templates is to increase the spatial resolution when computing water depths.

The wave spectrum analysis includes mainly the following two steps.

3.1.1. Spatial Fourier transformation

Since the wave changes its direction and wavelength as it propagates, the two-dimensional Discrete Fourier Transform (DFT) should be used to derive the wavenumber spectra from the satellite images. First, select a portion of the satellite image of $N \times N$ pixels (sub-image) with the pixel size equal to ΔX. Let X (m_1, m_2) represents the digital count of the pixel at (m_1, m_2). Then, we compute the DFT of this sub-image, which is defined as

$$F(n_1K_0, n_2K_0) = \frac{1}{N^2} \sum_{m_2=0}^{N-1} \left[\sum_{m_1=0}^{N-1} X(m_1, m_2) \mathrm{e}^{-in_1K_0m_1\Delta X} \right] \mathrm{e}^{-in_2K_0m_2\Delta X} \tag{3}$$

where

$D = N\Delta X$ ($\Delta X = 6.25$ m and $N = 64$ in this study)
n_1 and $n_2 = 1, 2, 3, \ldots, N$
$n_1K_0 = kx =$ wavenumber in the x direction
$n_2K_0 = ky =$ wavenumber in the y direction
$K_0 = 2\pi/D$ ($= 2\pi/400$ m for $N = 64$)

Limiting the choice of N to the power of 2, it permits the DFT computations by Fast Fourier Transforms (FFT). The power spectra were acquired in correspondence to the wavenumber in the x and y direction, respectively. The unit for the wavenumber coordinates kx and ky (Fig. 5) is $K_0 = 2\pi/400$ m.

3.1.2. Wavenumber spectrum

In a two-dimensional wavenumber spectrum, the spectral peak located at (n_x, n_y) represents characteristics of the dominant wave system which has the wavelength L and the wave direction θ (Leu et al., 1996):

$$L = 2\pi/k = 2\pi/(kx^2 + ky^2)^{1/2} = D/(n_x^2 + n_y^2)^{1/2} \tag{4}$$

$$\theta = \tan^{-1}(k_y/k_x) = \tan^{-1}(n_y/n_x) \tag{5}$$

3.2. Bathymetric mapping

The wavenumber spectrum analysis is performed on the wave image at both the reference area in the deep-water region and the study area of shallow water region near the coast. The wavenumber of the dominant wave system in the deep-water region can be used to derive its wavelength λ and frequency f through Eq. (2). When these waves propagate towards the coast, the shoaling effect shortens their wavenumber while keeping their

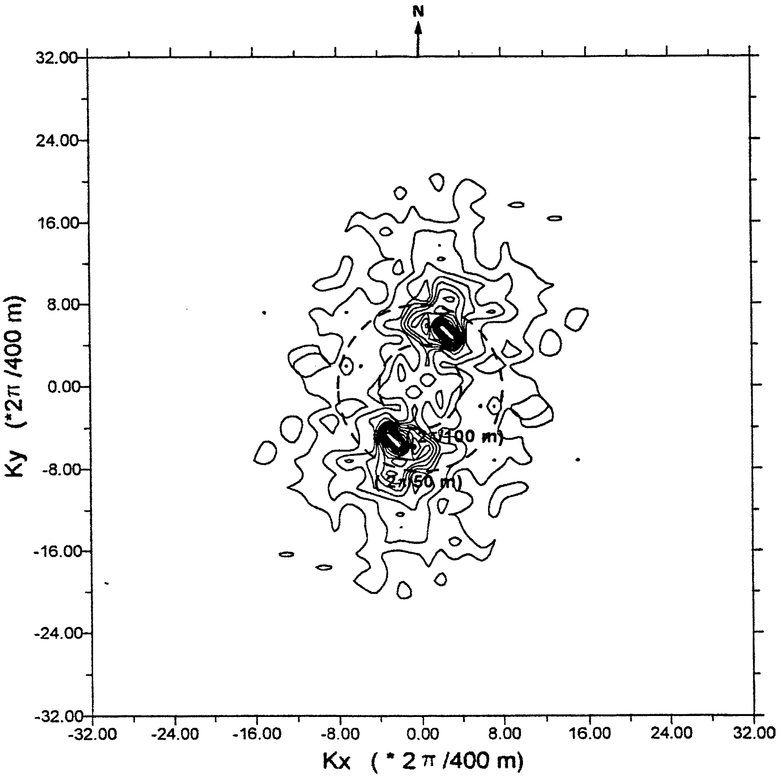

Fig. 5. Wavenumber spectrum (Case 1) of deep water derived from SPOT wave image. These contours of spectral power are in arbitrary unit.

frequency unchanged. Inserting the wavelength of the dominant wave system in the shallow water area and the frequency in the deep-water area into Eq. (1) of dispersion relation, we obtain the depth in the shallow water area.

To exemplify the procedure, a template is the basic unit of image in the spectrum analysis. The center of any template is the grid point. At each grid point, a template of 400 m by 400 m is formed with the neighboring four cells. The wavenumber vectors of dominant wave system and the water depth in each template (or at each grid point) are derived with the wave spectral analysis as described above. In order to reduce random errors of the derived water depths, equal weight moving average is applied to the 3×3 grid points. Bathymetric mapping using the spatial two-dimension image, this equal-weight moving average of 3×3 grid values is adopted in filtering of random noises (Kuo et al., 1999). That is the average of 3×3 grids values of water depth calculated and made as the new central value. Each new central grid value was obtained from moving and averaging the 3×3-grid shifting left-to-right and top-to-bottom over the grid system of 8×8. When the moving average was done, the 6×6 grids with new grid values were obtained from the 8×8 grids got rid of the boundary grids which were not really manipulated by moving average with neighbor grids. This smoothing procedure decreases the sensibility in detecting small-scale bathymetric fluctuation that may be unlikely in the accretion sandy coast of the study area.

3.3. Change detection and analysis

The information of water depths can be got from multi-temporal imageries manipulated by the WSB method. Maybe there is a notably seasonal, annual variation or instant variation of water depths after a special event such as a typhoon passed by or heavy rain and flow drainage with lots of sediment. The change of water depths should indicate where there is erosion or deposition over a given coastal zone. Comparing with in situ measured water depths, we calculate one and two standard deviations of water depths derived from multi-temporal imageries in every 2-m interval of water depth. Next, we calculate the difference of in situ measured water depths between two various temporal cases. One and two standard deviations of image-derived water depths present there are the confidence interval 68 and 95% to compare with in situ measured water depth in acceptable error. Also, comparing the difference of in situ measured water depths with one and two standard deviations of image-derived water depths, the probability and capacity of the change detection of imaged-derived water depths can be determined. By the way, we can estimate in quantity the difference of bed load accumulated over this study area and know where there is erosion or deposition in each cell of the grid.

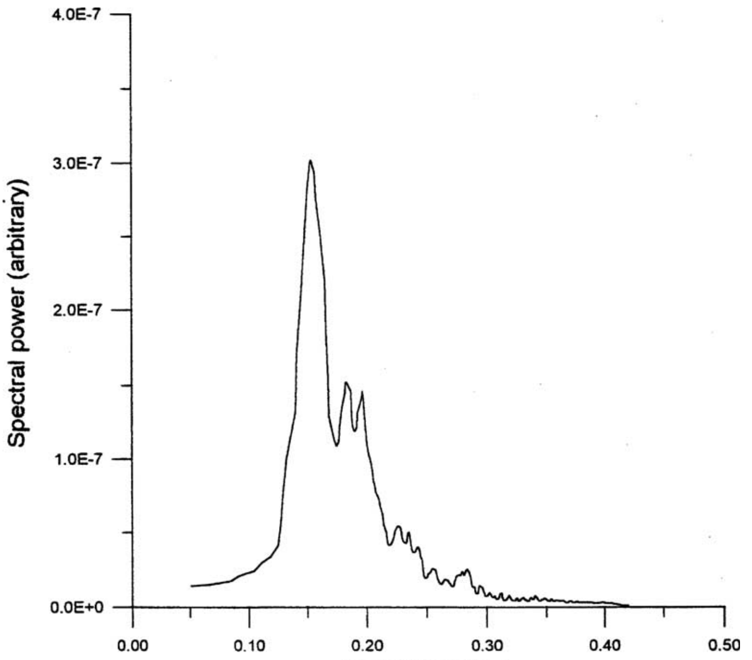

Fig. 6. Wave frequency spectrum (Case 1) of deep water derived from SPOT image indicates the spectral peak in 0.151 Hz.

3.4. Application of WSB method

The wave spectrum analysis described in Section 3.1 was applied to two SPOT 3 images over the coastal water in Taichung Harbor. Because of the high sedimentation in the area north of the harbor, we selected the region as the study area between the north groin and the north breakwater of Taichung Harbor.

3.4.1. Case 1

The image was taken at 10:45 a.m. of March 4, 1994. The wind data showed that the wind was 4.4 m/s from the north–northeast at 9:00 a.m., and was 4.1 m/s from the north–northwest at 11:00 a.m. This image in Fig. 2a shows the reference area of deep water

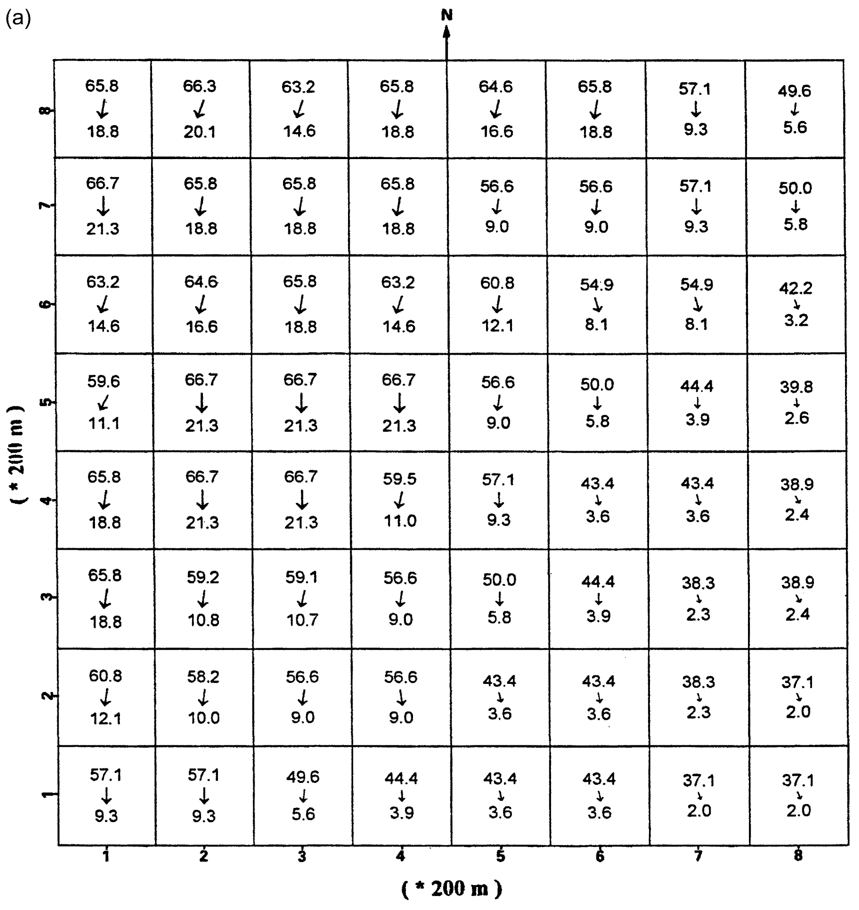

Fig. 7. (a) Case 1. The image-derived wavelengths (m) and water depths (m) at the grid points of study area. The north is in upward direction. The wavelengths and the water depths are listed above and below the arrows, respectively. (b) Case 2.

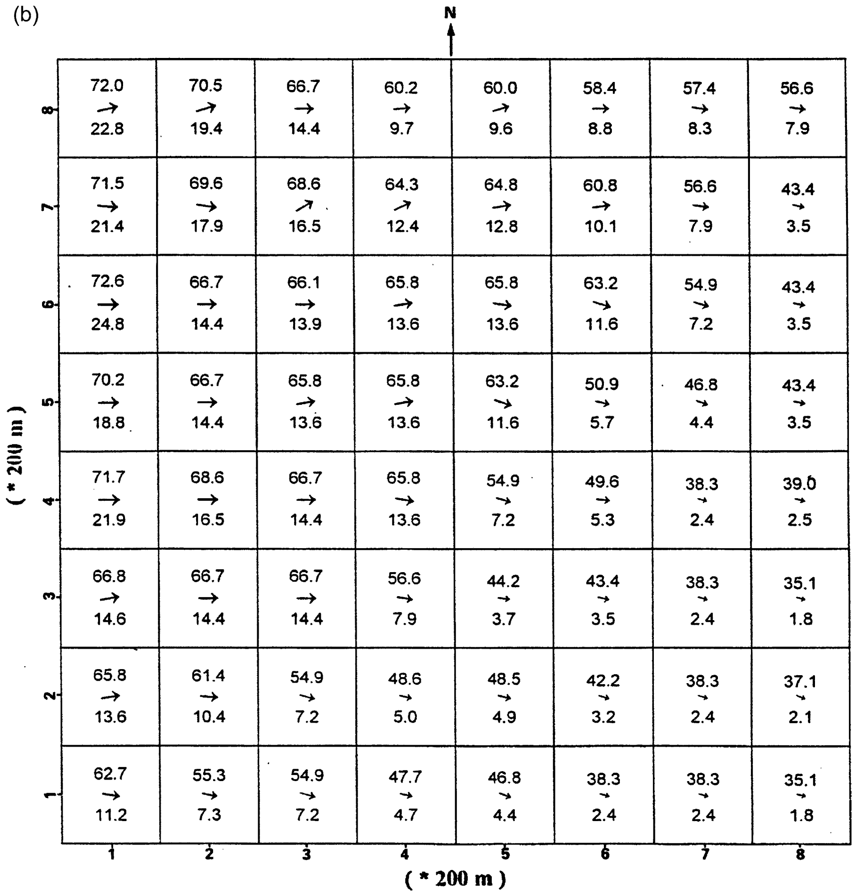

Fig. 7 (*continued*)

and the study area where depths are to be estimated by this method. This study area is located between the north groin and the north breakwater.

The reference area is of the size 800 m × 800 m, with depth about 50 m at 6–7 km offshore. The wave spectrum analysis was applied to the 400 m × 400 m sub-area. This wavenumber spectrum of deep water was derived and shown in Fig. 5. The dominant wave system located between the two concentric dash circles. The inner circle represents the wavelength of 100 m (i.e. wavenumber 2π/100 rad/m), and the outer circle represents the wavelength of 50 m (i.e. wavenumber 2π/50 rad/m). The wavelength of deep water was estimated to be about 69 m (see Fig. 5). The frequency of the dominant wave system was 0.151 Hz as shown in the frequency wave spectrum of Fig. 6.

Over the study area, the wave spectrum analysis was performed in the templates that are centered at the grid points, where the wavelength and the wave direction of dominant wave system can be determined from their spectral peaks to obtain the mean water depth.

To compare with the nautical charts, or with results from analysis on other images, one has to remove the tidal effect on the water depth. The tidal data showed that the sea level was 1.58 m above the reference level (the lowest low water level) when the SPOT satellite took the image on March 4, 1994. Fig. 7a shows the template-mean wavelength, wave direction, and the tide-corrected water depth at each grid point that is at the center of the template of 400 m×400 m. The original point (0,0) of coordinate system matches up to the low-left corner of the study area. Every wave characteristics at a grid point was derived from SPOT images in the template that centers at that grid point. At each grid point, the direction and the size of arrows represent the wave direction and the wavelength. The wavelength and the water depth

(* 200 m)	1	2	3	4	5	6	7	8
8	22.7	22.4	21.4	21.0	19.6	17.0	12.8	8.0
7	22.3	21.7	20.5	19.5	16.7	13.0	9.0	5.0
6	21.6	21.0	19.6	17.5	14.5	11.0	7.0	4.5
5	21.0	19.5	17.5	15.5	11.5	7.5	5.0	3.2
4	20.5	18.5	15.4	12.5	8.5	5.7	4.5	2.8
3	19.2	16.5	12.5	9.5	5.8	4.4	3.0	2.6
2	18.0	14.0	9.5	7.5	5.0	4.0	2.8	2.2
1	14.6	9.0	6.7	5.6	4.3	2.8	2.5	2.0

(* 200 m)

Fig. 8. The average in situ water depths (m) of 8×8 grids corrected for tidal elevation (Case 1, 1994). The coordinate system is the same as in Fig. 7.

are listed above and below the arrow, respectively. The water depth changed gradually from about 20 m at the upper left corner to about 2 m at the lower right corner. The pattern of arrows shows that water waves were propagating southward in the deep water, and they veered leftwards to the coast with shorter wavelength because of refraction.

3.4.2. Case 2

A SPOT 3 image (Fig. 2b) was taken at 10:45 a.m. of September 2, 1995. The wind data showed that the wind was 4.2 m/s from the northwest at 10:00 a.m., and was 4.6 m/s from the west at 11:00 a.m. The selection of reference area, the study area and the analysis procedures are the same as in Case 1. The wavelength and the frequency of the dominant wave system in the reference area were about 74 m and 0.145 Hz. Fig. 7b shows the wavelength and the wave direction of the dominant wave system, and the derived water depth of the study area. The waves propagated eastward and they veered rightwards to the shore at the lower right corner of the image. The wavelength becomes shorter in the shallower region.

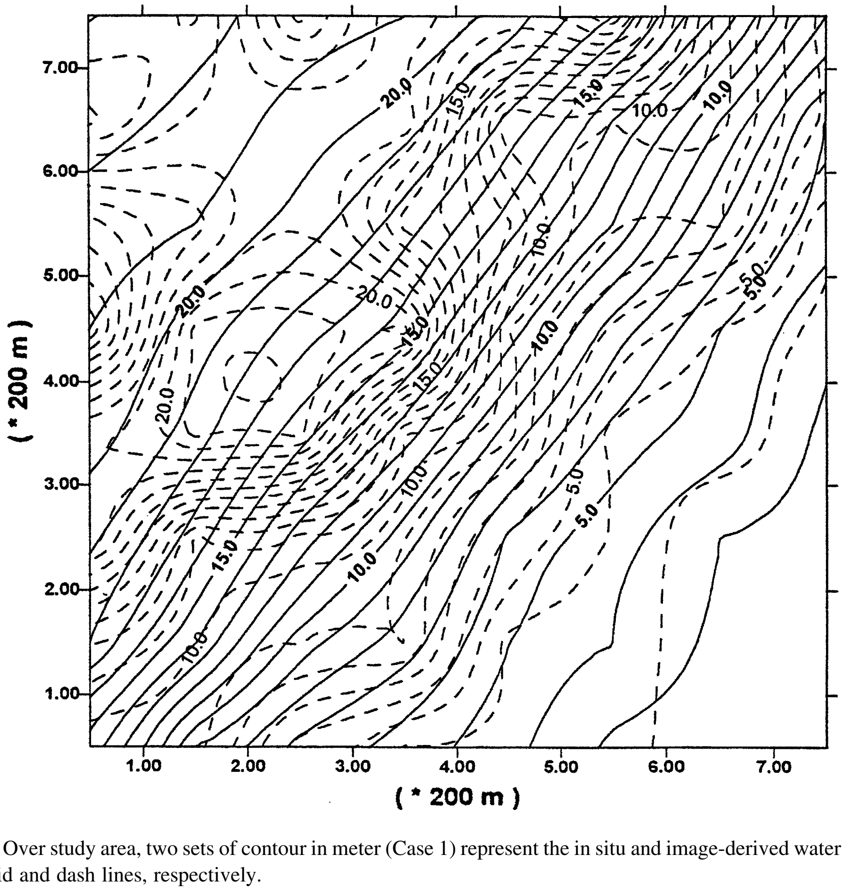

Fig. 9. Over study area, two sets of contour in meter (Case 1) represent the in situ and image-derived water depths by solid and dash lines, respectively.

To correct for tidal effect, the above image-derived water depths were also subtracted by 1.07 m as in Case 1. The derived water depth changes gradually from about 22 m at the upper left corner to about 2 m at the lower right corner. This bathymetry closely resembles that in Case 1 (SPOT image of March 4, 1994).

4. Comparison and verification

Both the wavelength and the wave direction were obtained through wave spectrum analysis of SPOT images. Assuming that the frequency is constant when water waves propagate from the deep water into the shallow water, the coastal water depth can be determined through the dispersion relation (Eq. (1)) of linear water waves. The question is that how accurate and how reliable the method is. The accuracy of the image-derived water depths will be estimated by comparison with in situ data measured by the shipboard echo sounder. As all sea level heights are referring to the mean lower low tide at Taichung Harbor, the actual water depth is the depth from the nautical chart plus the tidal elevation. The image-derived depth is an estimate of the actual water depth that varies with the tide.

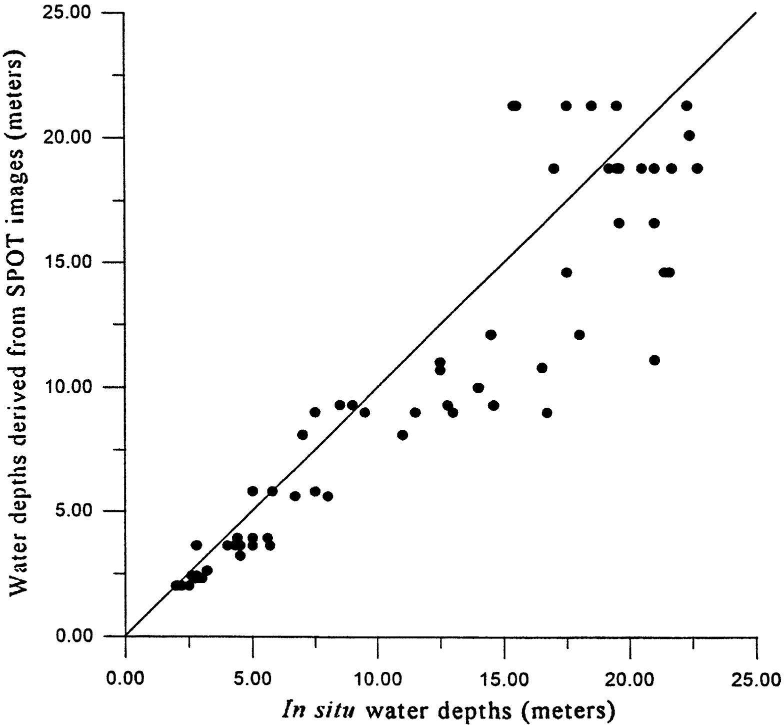

Fig. 10. Comparison between the SPOT image-derived water depths (without moving average) and in situ data (Case 1). The 45-degree oblique line represents the perfect fit.

4.1. Case 1

Fig. 8 shows the average in situ water depths corrected for the tidal elevation. The averaging was done over a template centered at each grid point of the study area. The deepest part is 22.7 m at the upper left corner, and the shallowest depth is 2.0 m at the lower right corner. For the convenience of comparison between these image-derived and in situ water depths, their contours were plotted together in Fig. 9. The original point (0,0) of coordinate system matches up to the low-left corner of the study area. The solid and dash lines represent the contours of in situ and image-derived water depths, respectively. Two sets of contours show reasonable agreement in the range of less than 12-m depth. The scatter plot (Fig. 10) of the image-derived water depth in Fig. 7a and the in situ measured water depths (Fig. 8) shows reasonable agreement—average error of 18.6% with a range of 0.3–47%. The 45-degree oblique line in Fig. 10 represents the perfect agreement between image-derived depths and the in situ measurements.

We found that the depth errors decreased significantly when the water was less than 12 m. There are two major factors for explanation of larger error in deeper water: (1) the wave in the deep-water region has much smaller influence from the sea bottom,

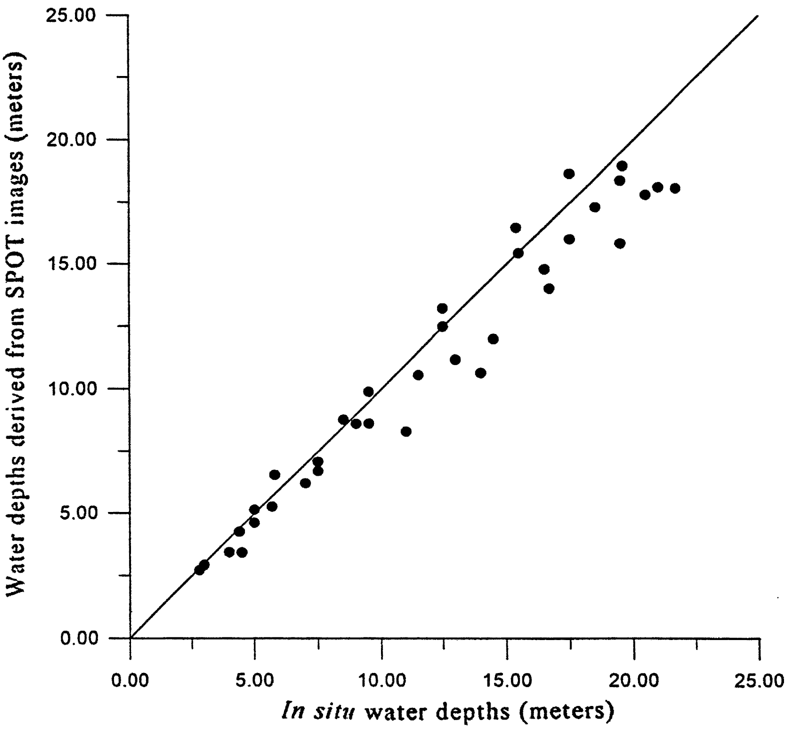

Fig. 11. Comparison between the moving averaged water depths derived from SPOT image and in situ data (Case 1). The differences of them converge at the 45-degree oblique line.

therefore, the satellite image cannot clearly show the change of bathymetry; (2) the number of waves in a 400 m×400 m template in the shallow water area increases because of shorter wavelength, then the determination of wavelength is more accurate (Kuo et al., 1999).

The sandy in the bottom north of Taichung Harbor has a smooth bottom, but the image-derived bathymetry has lots of bumps and dents. These random errors of the DFT-computed dominant wavenumber in the SPOT images and the derived water depth may come from the following sources:

(1) SPOT images are images of surface reflectivity which varies with the surface slope, the sun angle and the viewing angle of the satellite; the periodicity of the surface slope warrants power spectral peaks at the wavenumber of surface waves.

(* 200 m)	1	2	3	4	5	6	7	8
8	22.3	21.7	21.2	20.1	18.5	15.2	11.8	7.8
7	21.7	21.2	20.2	18.5	16.5	12.8	9.5	5.0
6	21.0	20.0	18.5	17.0	13.3	10.2	6.2	3.8
5	20.3	18.7	17.0	14.5	11.3	7.0	4.7	3.3
4	19.3	17.5	14.2	12.0	7.5	5.2	4.0	2.2
3	18.0	15.2	11.5	8.3	5.8	4.3	3.2	1.8
2	16.0	12.0	8.0	6.2	4.5	3.5	2.2	1.7
1	12.0	7.2	5.8	4.7	3.6	2.7	2.1	1.5

(* 200 m)

Fig. 12. The averaged in situ water depths (m) of 8×8 grids over the study area (Case 2, 1995). The coordinate system is the same as in Fig. 7.

(2) However, the surface reflectivity increases greatly with randomly distributed white caps near wave crests. Therefore, the presence of white caps increases the indeterminacy of dominant wavenumber.

The filtering of random noises in the derived water depth data is done by equal-weight moving average of 3×3 grid points to obtain the smoothed depth in the central 6×6 grids for comparison with the in situ water depths. The improvement in correlation is significant, as shown in Fig. 11. The average error was reduced to 9.70%. The errors range from 0.16 to 24%, much less than that, i.e. 47%, before smoothing.

4.2. Case 2

Due to the success in filtering out the noise in the depth data of Case 1, we perform the same smoothing process on the derived depth data of Case 2. The in situ water depths are shown in the 8×8 grids of Fig. 12. Although both Figs. 8 and 12 cover the same region,

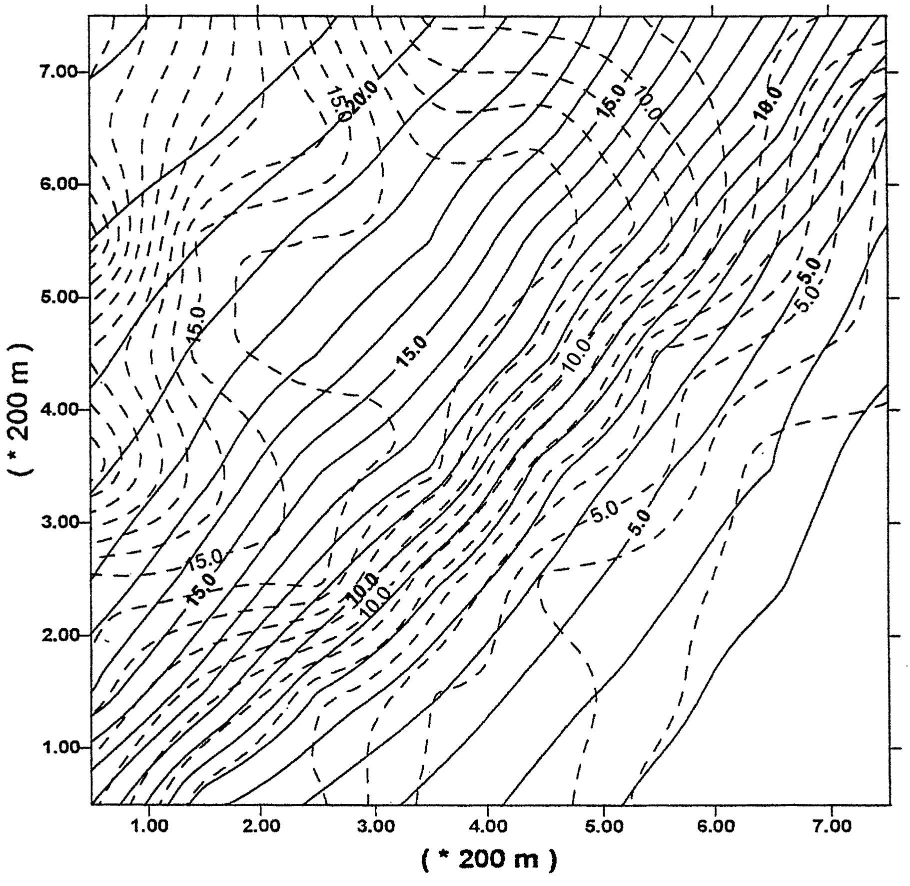

Fig. 13. As in Fig. 9 for Case 2.

they are in situ measurement of water depth in 1994 and 1995, respectively. The heavy sedimentation near the Taichung results in the change of bathymetry. The image-derived water depth in Fig. 7b agrees well with those in Fig. 12. The average error of the image-derived water depth is 16.19% with a range from 0.6 to 52%. Plotting their contours together in Fig. 13, the solid and dash lines represent the contours of in situ and image-derived water depths, respectively. This figure shows both of their contours fine agreement in the range of less than 10-m depth and reasonable agreement in the maximum range not beyond 12-m depth. In addition to the random errors mentioned in the Case 1, there are ship wakes contaminating the wave field in the upper portion of the study area. After applying the same filtering procedure as in Case 1, the average error is improved to be 11.12% with the maximal error of 31%. Like Figs. 10 and 11, the scatter plots of image-derived water depths vs. in situ measurement for Case 2 are shown in Figs. 14 and 15, respectively. As in Case 1, the accuracy of image-derived water depth is better in the region shallower than 12 m.

Comparison between image-derived water depths and in situ measurement of water depths, the average errors are 9.7 and 11.12% in cases 1994 and 1995, respectively. Shown as Fig. 16, the differences of water depths during 1994–1995 are calculated from image-derived water depths and in situ data. Both values listed above and below in each cell are in

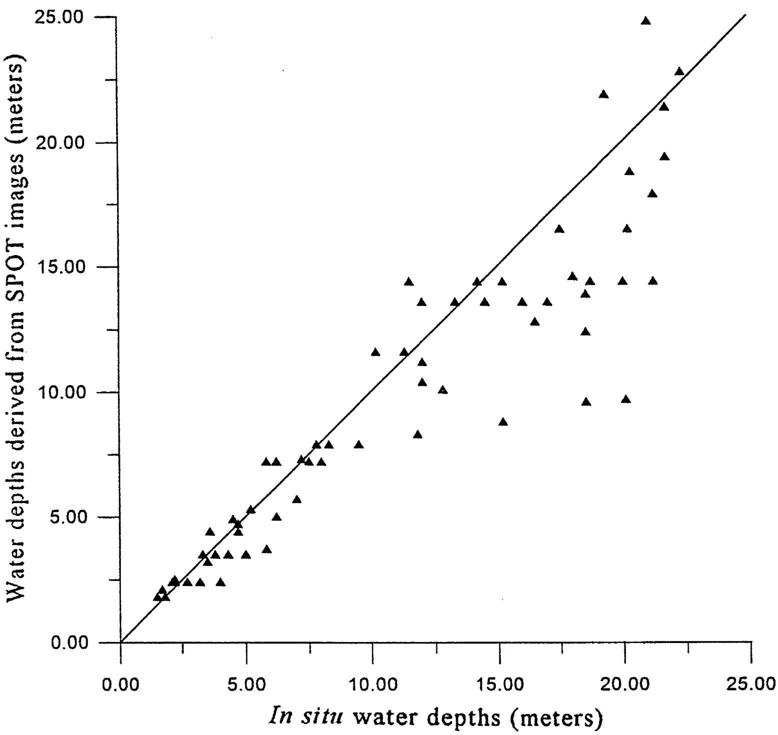

Fig. 14. Comparison between the SPOT image-derived water depths (without moving average) and in situ data (Case 2).

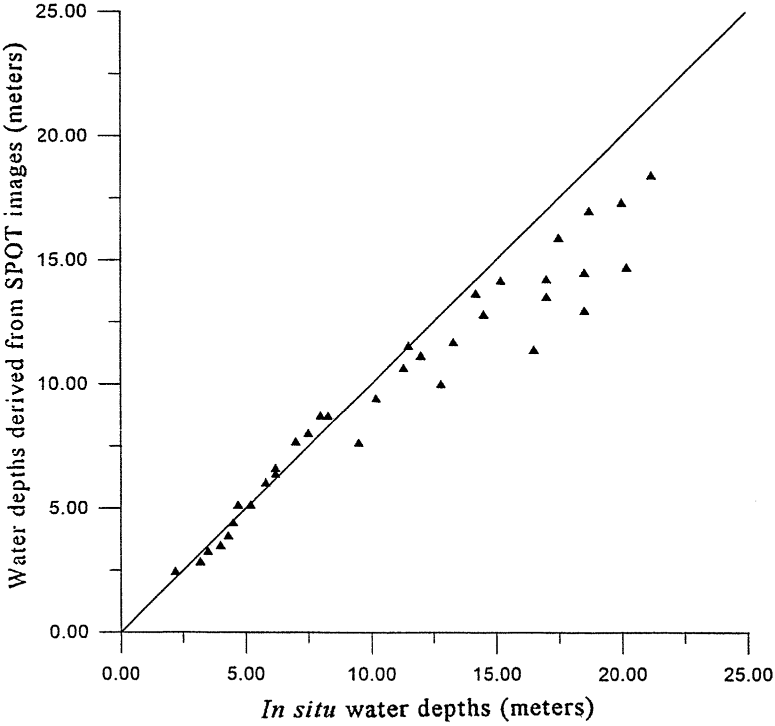

Fig. 15. Comparison between the moving averaged water depths from SPOT image and in situ data (Case 2).

meter. They were derived from image-derived water depths and in situ data, respectively. Fig. 16 shows that the 6×6 grids obtained from 8×8 grids got rid of the boundary cells. The cell size is 200×200 m. From change analysis of image-derived water depths, the study area between the groin and the breakwater was almost deposited by sand drift except three up-right cells and the low-left one. This result agreed well with that obtained from in situ measurement and calculation. Furthermore, this research wants to know the capacity and probability of change detection of water depths by calculating and analyzing the differences of water depths in 1994 and 1995.

To fundamental hypothesis, assume the change of water depths as the normal distribution. Confidence intervals and probability statements (their definitions see Bendat and Piersol, 1986) according to the normal distribution are adopted in the following analysis. At first, calculate the differences of image-derived water depths and in situ ones in both consecutive years. Then, calculate one and two standard deviations for the differences of image-derived water depths at every interval of 2-m water depth. At the confidence intervals regarding one and two standard deviations, it has 68 and 95% confidence to remotely sense and estimate the differences of water depths in both 2 years. In Fig. 17, there are two disjunctive lines indicating the acceptable errors of one and two standard deviations calculated from image-derived water depths in 1994 and 1995. Each triangle dot presents the difference of in situ water depths in 1994 and 1995. Comparing

0.15 + 1.01	3.58 + 0.81	3.35 + 1.51	3.12 + 0.71	1.65 + 0.71	1.44 + 0.01
1.27 + 1.51	4.94 + 1.61	2.96 + 1.01	0.80 + 1.71	–0.67 + 1.31	0.32 + 1.31
1.87 + 1.31	4.89 + 1.01	3.12 + 1.51	0.39 + 0.71	–0.11 + 1.01	–0.03 + 0.81
1.88 + 1.51	3.30 + 1.71	2.58 + 1.01	1.23 + 1.51	0.61 + 1.01	0.39 + 1.01
1.10 + 1.81	1.43 + 1.51	1.66 + 1.71	1.00 + 0.51	0.83 + 0.61	0.56 + 0.31
–0.02 + 2.51	0.37 + 2.01	0.59 + 1.81	1.20 + 1.01	0.65 + 1.01	0.74 + 1.11

Fig. 16. Water-depth differences in study area in both cases 1994 and 1995. Both values listed above (image-derived) and below (in situ data-derived) in each cell are in meter.

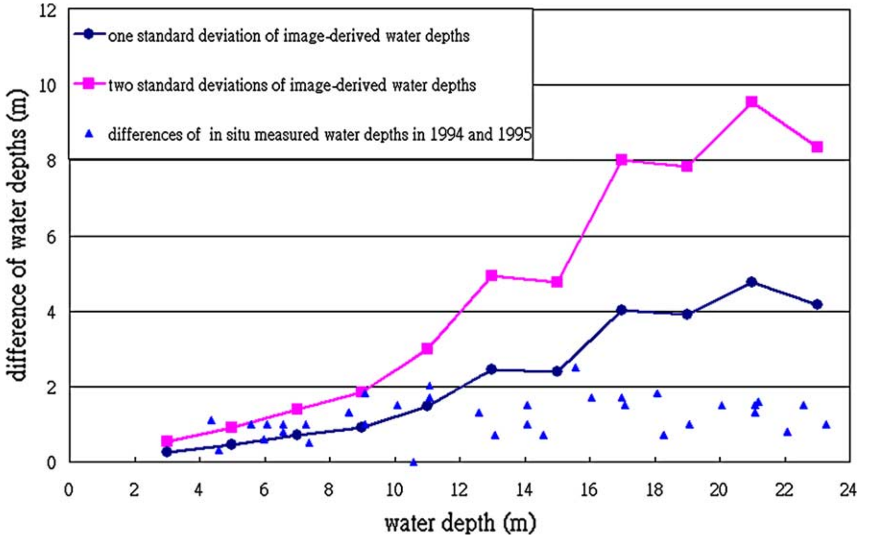

Fig. 17. Change detected analysis of water depths derived from both variously temporal imageries 1994 and 1995.

with the difference of in situ measured water depths in both years, there are almost all triangle dots plotted above the disjunctive line of one standard deviation but below another line of two standard deviations. This shows when the water depth is less than 12 m, there is more 68% and less 95% of confidence and probability to detect the water-depth change of this study area in both cases 1994 and 1995 by remote sensing and imageries analysis. Being alternate statement, evidence shows the differences of in situ water depths are less than one standard deviation of image-derived ones when the water depth is deeper than 12 m. This also means that the change detection of remote sensing depth is less 68% confidence when the water depth is deeper than 12 m.

As contours shown in Figs. 18 and 19 obtained from imageries analysis and calculation of in situ data, respectively, they present the differences of bed load in 1994 and 1995 accumulated and distributed over the study area. In the low-right part of study area, there is a good agreement of differences of bed load estimated from both imageries data and in situ ones. Comparing with Figs. 18 and 19, the remotely sensing and estimation of differences of bed load shows that the more accurate the difference of bed load becomes, the shallower

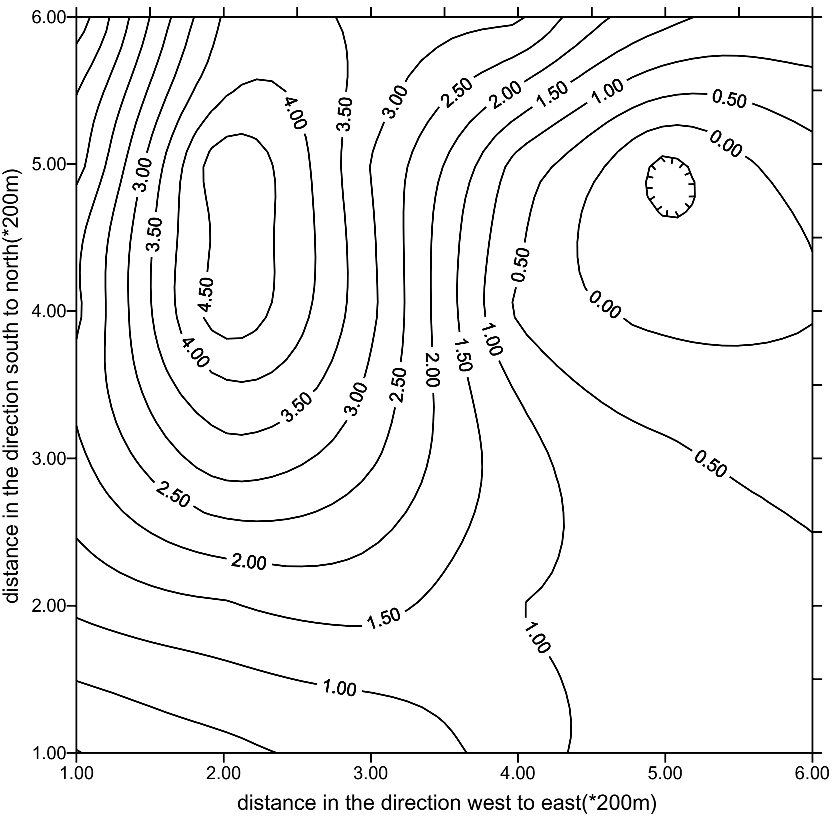

Fig. 18. Contours of difference of image-derived bed load (m^3) on the 6×6 grids.

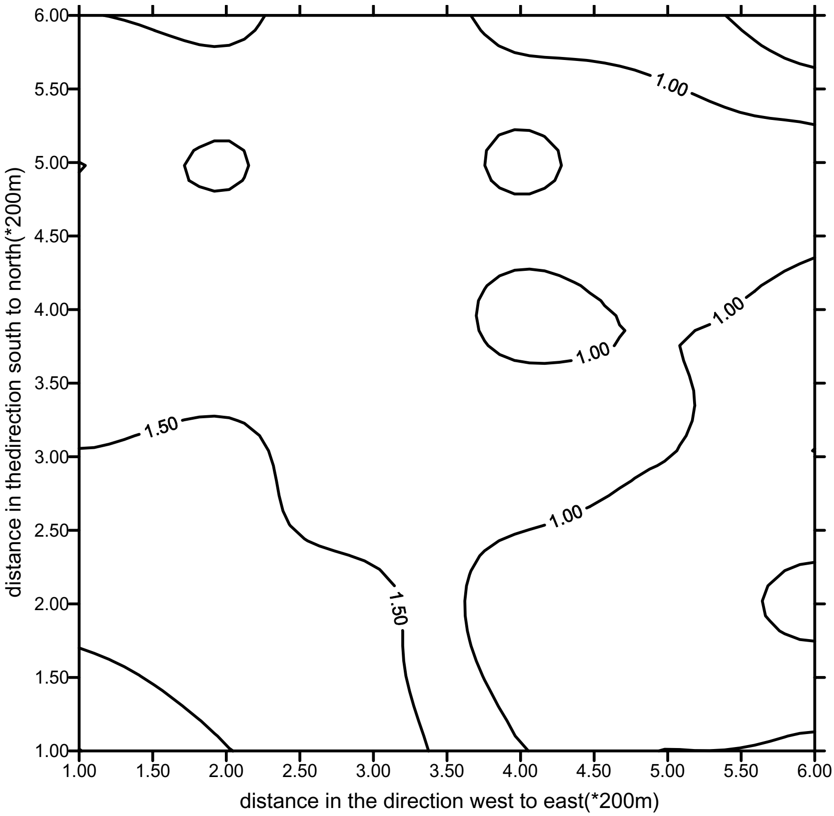

Fig. 19. Contours of difference of in situ measured bed load (m^3) on the 6×6 grids.

the water depth goes. Being deeper than 12 m, there is not a good agreement in the difference of bed load derived from satellite imageries and in situ data.

5. Discussion and conclusion

This study analyzes the wave fields of two SPOT images in the consecutive years of 1994 and 1995. The wave spectrum bathymetric (WSB) method was adopted to derive the wavelength and the wave direction from SPOT images, thereafter derive the water depth in the coastal zone. The assumption is that wave propagates from the deep to shallow water without changing its frequency. The error of the image-derived water depth is 18.6% in Case 1 (1994) and 16.2% in Case 2 (1995).

This method is well suited for the western coast of Taiwan where the water quality and the sea floor characteristics have large spatial variation and therefore adversely affect the optical bathymetry method. Comparing the image-derived water depths (see Fig. 7a and b) with in situ ones (see Figs. 8 and 12), comparison dots of water depth (Figs. 10, 11, 14, and 15) apparently shift apart from the 45-degree oblique line when the water depths are more than 12 m. The depth errors are at the range of 0–2 m when the water depths are less than 12 m, but the errors are more than 2 m when they are deeper than 12 m. Figs. 11 and 15 also illustrate the depth errors increased significantly when the water depths are deeper than about 12 m. Based on the evidence, the depth errors less than about 2 m can be regarded as the criteria to confirm the good depth estimation by WSB method in the cases study. This study finds that the WSB method is less accurate over regions deeper than about 12 m in the cases study. Generally this conclusion is acceptable using about ‘12 m’ as the critical point for the better validity of WSB method. This conclusion is similar to the other case study using QuickBird imagery (Leu, 2004). These phenomena may result from that (1) the dispersion relation is less sensitive to the water depth in the deep-water region, and (2) there are enough numbers of waves to get better wavelength resolution in the shallow water region. Acceptably accurate water depths may be derived from using the dominant wave system of wavelength 70 m or longer over the depth of 12 m or less. Also, the larger template has the result of poor spatial resolution of the bathymetry, but it gives better wavelength resolution if the wavelength is uniform in the template. This assumption is less valid in regions of large change of bathymetry, e.g. the study area north of Taichung Harbor (Fig. 2). Therefore, the size of template should be as small as possible comparing to bathymetry, but as large as possible comparing to the wavelength of the dominant waves.

In addition, adopting overlapping templates (Fig. 4) and moving average (Figs. 11 and 15) helped reducing random errors in the image-derived water depth while sacrificing little on the spatial resolution of the derived water depth. The average error of the image-derived water depth may be reduced to about 10% after moving average in case study. The moving average procedure may be replaced by using larger templates to simplify the WSB analysis, if the wave spectra (and the water depth) change little from templates to templates. But, there will be indeterminacy of dominant wavenumber in regions where wave spectra changes greatly from one template to the next, and hence the depth changes drastically from one template to the next. For example, in the lower-center portion of Fig. 8, tripling the size of templates (corresponding to 3×3 moving average of depth data in Figs. 11 and 15) will force the WSB analysis to select a water depth from 2.8 to 9.5 m. We therefore prefer the current size of templates where depth changes within a cell are of the order of 20%, to near 100% if the size is tripled.

In change detection and analysis of water depths and bed load using satellite imageries, this result of cases study indicates that the confidence of detecting water-depth change in the region is above 70% when the water depths are less than 12 m. Also, analyzing multi-temporal imageries, it gets the same confidence in change detection of bed load accumulated over the region shallower than 12 m. This wave spectrum bathymetric method is particularly useful for places that are difficult to reach and for regions where bathymetry changes drastically every year. Airborne images and the soon-to-come higher resolution satellite images are expected to further improve the accuracy of this method in determining the bathymetry of coastal waters. Also, this WSB method is expected to improve the confidence of change detection of water depth and be really assumed where there is erosion or deposition in coastal zone.

Acknowledgements

Be grateful to the Center of Harbor and Marine Technology of Taiwan province for providing various information and data on wind, tide and water depth, etc.

References

Alpers, W., Hennings, I., 1984. A theory of the imaging mechanism of underwater bottom topography by real and synthetic aperture radar. Journal of Geophysical Research 89 (C6), 10529–10546.

Beal, R.C., 1980. Spaceborne imaging radar: monitoring of ocean waves. Science 208, 1373–1375.

Bendat, J.S., Piersol, A.G., 1986. Random Data Analysis and Measurement Procedures. Wiley, London p. 566.

Cox, C.S., Munk, W.H., 1954. Statistics of the sea surface derived from sun glitter. Journal of Marine Research 13, 198–227.

Hengel, W.V., Spitzer, D., 1991. Multi-temporal water depth mapping by means of Landsat TM. International Journal of Remote Sensing 12 (4), 703–712.

Kasischke, E.S., Shuchman, R.A., Lyzenga, D.R., 1983. Detection of bottom features on SEASAT SAR imagery. Photogrammetric Engineering and Remote Sensing 49 (9), 1341–1353.

Kuo, Y.Y., Leu, L.G., Kao, Y.L., 1999. Directional spectrum analysis and statistics obtained from ERS-1 SAR wave images. Ocean Engineering 26, 1125–1144.

Leu L.G., 1998. Spectrum analysis of ocean surface wave and coastal water depths derived from satellite images. PhD dissertation. National Chiao Tung University, Taiwan, ROC (in Chinese).

Leu L.G., 2004. Bathymetric mapping in kending shallow waters using a QuickBird imagery. Journal of Photogrammetry and Remote Sensing 9 (2), 23–42, (in Chinese).

Leu, L.G., Kou, Y.Y., Liu,, C.T., 1996. Examples of ocean wave spectral estimated from ERS-1 SAR images. La mer 34 (2), 45–55.

Tripathi, N.K., Rao, A.M., 2002. Bathymetric Mapping in Kakinada Bay, India, Using IRS-ID LISS-III Data. International Journal of Remote Sensing 23 (6), 1013–1025.

Vesecky, J.F., Stewart, R.H., 1982. The observation of ocean surface phenomena using imagery from the SEASAT synthetic aperture radar: an assessment. Journal Geophysics Research 87, 3397–3430.

Vogelzang, J., 1992. Sea bottom topography with X-band SALR: the relation between radar imagery and bathymetry. International Journal of Remote Sensing 13 (10), 1942–1958.